J Mol Model (2006) 12: 931–941
DOI 10.1007/s00894-006-0102-6

ORIGINAL PAPER

Wely B. Floriano · Spencer Hall · Nagarajan Vaidehi · Unkyung Kim · Dennis Drayna · William A. Goddard III

Modeling the human PTC bitter-taste receptor interactions with bitter tastants

Received: 27 September 2005 / Accepted: 16 January 2006 / Published online: 11 April 2006

Abstract We employed the first principles computational method *MembStruk* and homology modeling techniques to predict the 3D structures of the human phenylthiocarbamide (PTC) taste receptor. This protein is a seven-transmembrane-domain G protein-coupled receptor that exists in two main forms worldwide, designated taster and nontaster, which differ from each other at three amino-acid positions. 3D models were generated with and without structural similarity comparison to bovine rhodopsin. We used computational tools (*HierDock* and *ScanBindSite*) to generate models of the receptor bound to PTC ligand to estimate binding sites and binding energies. In these models, PTC binds at a site distant from the variant amino acids, and PTC binding energy was equivalent for both the taster and nontaster forms of the protein. These models suggest that the inability of humans to taste PTC is due to a failure of G protein activation rather than decreased binding affinity of the receptor for PTC. Amino-acid substitutions in the sixth and seventh transmembrane domains of the nontaster form of the protein may produce increased steric hindrance between these two α-helices and reduce the motion of the sixth helix required for G protein activation.

Keywords Phenylthiocarbamide · Bitter · Protein structure · G Protein-coupled receptor · Taste perception

W. B. Floriano
Biological Sciences Department,
California State Polytechnic University Pomona,
Pomona, CA 91768, USA

S. Hall · N. Vaidehi · W. A. Goddard III
Materials and Process Simulation Center (MSC),
California Institute of Technology,
Pasadena, CA 91125, USA
e-mail: wag@wag.caltech.edu

U. Kim
Department of Biology, Kyungpook National University,
Daegu 702-701, Republic of Korea

D. Drayna (✉)
National Institute on Deafness and Other Communication Disorders, National Institutes of Health,
5 Research Court,
Rockville, MD 20850, USA
e-mail: drayna@nidcd.nih.gov
Tel.: +1-301-4024930
Fax: +1-301-8279637

Introduction

The T2R mammalian taste receptors are seven-transmembrane (TM) domain G protein-coupled receptors (GPCRs) [1, 2]. Extracellular bitter substances bind to these receptors and initiate neural signaling via activation of intracellular heterotrimeric G proteins [3]. Despite numerous studies on taste receptors, there remains a great deal of uncertainty in what characteristics of the molecules govern the perception of taste. Particularly interesting clues are given by the human taste sensitivity to the bitter compound phenylthiocarbamide (PTC), which for some individuals is intensely bitter, but for others is largely tasteless. Intense studies performed since this phenomenon was discovered in 1932 [4] have determined that this difference in perception is genetically determined. In particular, three single-nucleotide polymorphisms (SNPs) in a TAS2R/T2R bitter receptor (PTCR) [5] are responsible. These SNPs result in the mutations Pro49 to Ala (P49A), Ala262 to Val (A262V), and Val296 to Ile (V296I). Two predominant haplotypes of the gene encode two major forms of the protein, and these PAV (taster) and AVI (nontaster) forms account for the majority of PTC taster and nontaster individuals in the worldwide population [5, 6].

The bimodal distribution of tasters/nontasters observed for PTC is also observed for the structurally related compound 6-*n*-propylthiouracil (PROP) [4, 7, 8], and hence both compounds are commonly used in psychophysical studies. In addition, a large number of different compounds that share the N─C=S moiety with PTC and PROP also show that polymorphic sensitivity in humans', and within individuals', taste sensitivity to all of these compounds is strongly correlated [9, 10].

Extensive studies have been performed on the sensory physiology of bitter taste, and variation in sensitivity to a wide variety of other bitter substances has been noted, including quinine, epicatechin, tetralone, urea, sucrose octaacetate, denatonium benzoate, caffeine, L-phenylalanine, and L-tryptophan [11]. The degree to which differences in the PTC receptor might affect these other tastes is not understood. Psychophysical studies have demonstrated that smokers and coffee or tea drinkers tend to be nontasters [12, 13], suggesting that bitter compounds present in cigarettes, coffee, and tea may compete with PTC for the same bitter receptors. Such data suggest that PTC taster status correlates with a number of behaviors with important health implications. In fact, the ability to taste the bitter compounds PTC and PROP was found to be a protective factor against cigarette smoking [14]. On the other hand, PTC tasters may perceive vegetables such as cauliflower, cabbage, broccoli, and Brussels sprouts as unpleasantly bitter. These vegetables contain isothiocyanates, chemical compounds closely related to PTC, found to have medicinal and pharmacological properties as antitumor and anti-inflammatory agents [15]. While nontasters may be more susceptible to smoking, tasters may avoid consuming beneficial nutrients, both with negative impact on the individual's health. PTC tasters may also find some medicinal drugs too bitter and they may resist taking them, which is potentially an issue with very young children.

In comparison to other GPCRs, the variant amino acids in the two forms of the PTC receptor were predicted to reside in the first intracellular loop, the sixth TM, and the seventh TM of this protein. However, the precise location of these variants in the protein structure and the molecular details of how these alterations cause changes in receptor function have remained unknown.

As a first step in obtaining a better understanding of how the differences in molecular structure of the tastants and mutations in the PTC affect signal transduction, we used homology modeling and the recently developed *MembStruk* [16–18] methods to predict the 3D tertiary structures for the PTC bitter receptor haplotypes PAV (taster) and AVI (nontaster).

We then used the *HierDock* first principles method [16, 17, 19] to predict the binding site and binding affinity for 12 bitter compounds (PTC, atropine, brucine, chloroquine, naringin, quinacrine, quinine, salicin, caffeine, nicotine, epicatechin, and cycloheximide) to the 3D structure of each form of the receptor. Based on the analysis of the 3D structures for the bitter compounds bound to the PTC receptor and their binding profiles, we propose an explanation for the observed correlation between taste ability and haplotypes.

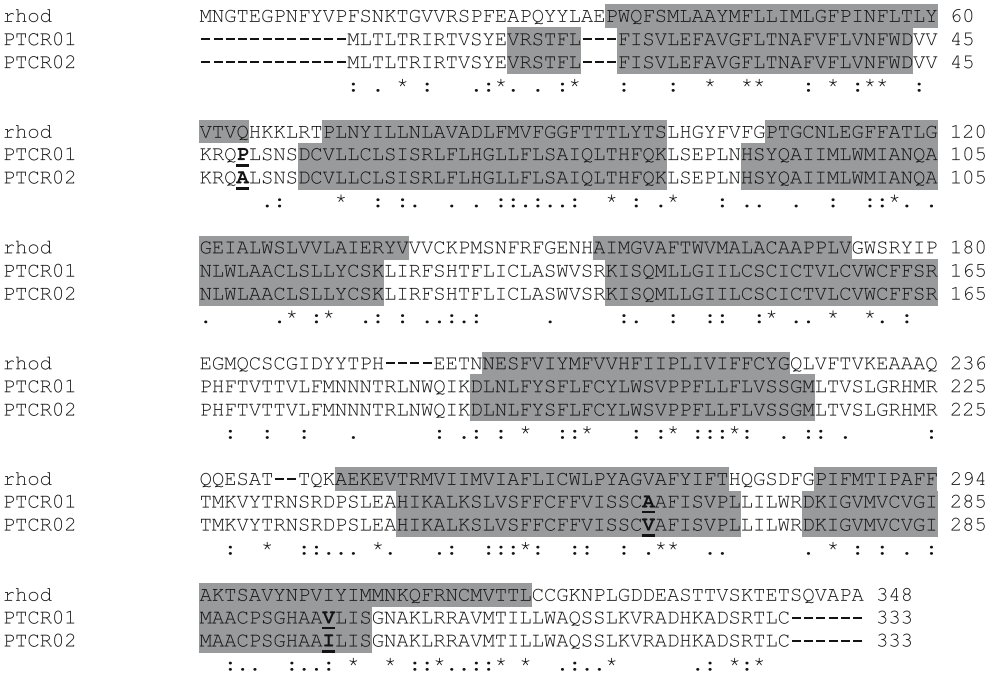

Fig. 1 MembStruk 3.5 secondary structure prediction (*shaded segments*) and sequence alignment against bovine rhodopsin (*rhod*) for phenylthiocarbamide receptor variants PTCR01 (taster) and PTCR02 (nontaster). The secondary structure assignment for rhodopsin was taken from the pdb file (1L9H). To predict the MembStruk TMs, we used a set of 12 taste receptors (UniProt entries Q9NYV8, Q9NYV9, Q9NYW1, Q9NYW3, Q9NYW2, Q9NYW0, Q9NYW6, Q9NYW7, Q9NYW4, Q9NYW5, Q9NYV7, Q9P1R1) plus PTCR01 and PTCR02 (sequence alignment not shown). The TMs predicted by MembStruk were used to build 3D structures PTCR01a, PTCR01b, and PTCR01d, as described in the "Materials and methods". The bovine rhodopsin structure 1L9H was used to build the homology-based 3D model (PTCR01c)

Materials and methods

3D structures for bitter compounds

The chemical structures of the bitter compounds (PTC, atropine, brucine, chloroquine, naringin, quinacrine, quinine, salicin, caffeine, nicotine, epicatechin, and cyclohexamide) were drawn using ISIS DRAW [20] and saved as a "mol" file format. We used the program Concord [21], which reads the mol file and generates 3D coordinates, to add hydrogen atoms and assign Gasteiger atomic charges [22]. The Concord-generated ligands were energy-minimized to a root mean square deviation (RMS) force of 0.2 kcal mol^{-1} $Å^{-1}$ in gas phase using conjugate-gradient minimization and the Dreiding force field [23]. These minimized structures were then used for docking.

3D structures for the PTC receptor

MembStruk [16–18] version 3.5 was used for de novo protein structure prediction. The homology-based models were generated using the programs Quanta [24] and Whatif [25] and the sequence alignment shown in Fig. 1. All receptor models were energy-minimized to an RMS force of 0.2 kcal mol^{-1} $Å^{-1}$ using the Dreiding force-field [23] and CHARMM22 [26] charges.

Scanning for possible binding site(s)

For each of the eight 3D structures described in the "Results" section (four for the taster variant and four for the nontaster variant), we used the *ScanBindSite* protocol to scan independently for potential binding sites using PTC as probe. The main steps of this protocol are as follows:

1. Find the centers for empty pockets in the entire available volume of the receptor using the program Pass [27].
2. Define the scanning regions as 10 Å around those centers.
3. Generate and score multiple bound configurations of the probe ligand(s) into each scanning region.
4. Eliminate configurations that have less than 90% of the ligand molecular surface buried by the protein surface.
5. Select based on energy the best configuration among all regions for each probe ligand. These will define the location of the putative binding site to be used for predicting binding modes and binding affinities.

Predicting binding modes and binding affinities

We used the HierDock [16, 17, 19] first principles method technique to predict the binding site and binding energy of each ligand to the PTCR 3D models. HierDock has been used previously to predict the binding site for epinephrine to the β1 and β2 adrenergic receptors [17, 28], for alcohols to the S25 mouse olfactory receptor (OR) [16], and for a series of odorants to several other ORs [29].

Results

Predictions of the tertiary structure

We used four different strategies to build computational 3D models for the two variants of the PTC receptor. In each case, the taster variant was built first and then mutated to the nontaster variant. The four strategies used were as follows:

(a) We used the MembStruk protocol version 3.5 [18] to predict the TM domains and the 3D structure of the receptors. The TM domains were predicted using an alignment of 12 human taste receptors (UniProt entries Q9NYV8, Q9NYV9, Q9NYW1, Q9NYW3, Q9NYW2, Q9NYW0, Q9NYW6, Q9NYW7, Q9NYW4, Q9NYW5, Q9NYV7, Q9P1R1) plus the two PTC haplotypes. The resulting structures are identified as PTCR01a and PTCR02a.

The amino-acid sequence and 3D structure of bovine rhodopsin were not used in this strategy for predicting the PTCR structures.

(b) Starting with the structures obtained in (a), we optimized the rotations and translations of the helices with respect to each other by searching for Cys bridges that could be formed with small rotations and/or translations of the TMs carrying the potential Cys pairs. The Cys pairs within a reasonable Cys–Cys distance in the 3D models from (a) found in this step are: C59(TM2)–C112(TM3), C254(TM6)–C289 (TM7), and C261(TM6)–C282(TM7). These resulting structures are identified as structures PTC01b and PTC02b.

(c) To determine how well the first principles MembStruk approach compares to standard homology modeling for determining the 3D structure of a GPCR, we built a homology-based 3D model for both receptors using the crystal structure of bovine rhodopsin (PDB code 1L9H, GenBank accession K00506) using the programs Quanta [24] and Whatif [25]. The ClustalW [30] alignment used to generate the model is shown in Fig. 1. The sequence similarity and identity between bovine rhodopsin and PTC01 are 25 and 10%, respectively. These homology-based structures are referred to as PTC01c and PTC02c throughout the text.

(d) Finally, we built a hybrid structure that combines the TM segments from 1L9H (without loops and without the eight rhodopsin helices) with the TM predictions from (a) and the rotation/translation approach from (b). This leads to the Cys154(TM4)–Cys198(TM5) pair in addition to the three pairs listed in (b). We shortened or lengthened the rhodopsin TMs to fit the TM predictions obtained through MembStruk, and then added loops and optimized the structures using the proce-

dures in the MembStruk protocol. The resulting structures are denoted as PTCR01d and PTCR02d.

Figure 1 shows the sequence alignment between PTCR01, PTCR02, and rhodopsin (used for the homology modeling). The TM domains defined in the crystal structure are shaded in the rhodopsin's sequence. The TMs predicted by MembStruk 3.5 (shaded segments in the PTCRs sequence) were used to build the 3D structures (a), (b), and (d). Figure 2 shows the four 3D model types with the Cys bridges differentiating structures (a) and (b), and the Cys bridges for model (d). Table 1 lists the RMS in coordinates for the alpha Carbon atoms (CRMS) in TM segments among the 3D models. The CRMS between each pair of taster and nontaster structures was less than 0.15 Å in all four cases.

General location of the putative binding site(s)

To determine the location of the potential binding sites for the various tastants, we used the ScanBindSite computational procedure [16, 17] for each of eight (four taster variants and four nontaster variants to each of the eight) 3D structures of PTCR. The results are shown in Fig. 2. Structures (a) (MembStruk 3.5) and (c) (homology to 1L9H rhodopsin crystal structure) have the binding site in equivalent regions, between TMs 3, 4, 5, and 6. This location is consistent with the binding site for retinal in bovine rhodopsin [31]. Structures (b) and (d) [with helices rotated, respectively, from (a) and (b)] have their binding sites shifted towards TMs 1 and 7 [structure (b)], and TM4 [structure (d)]. Figure 3 shows, as solid sphere clusters, the various scanning regions found in PTCR01 structures (a) to

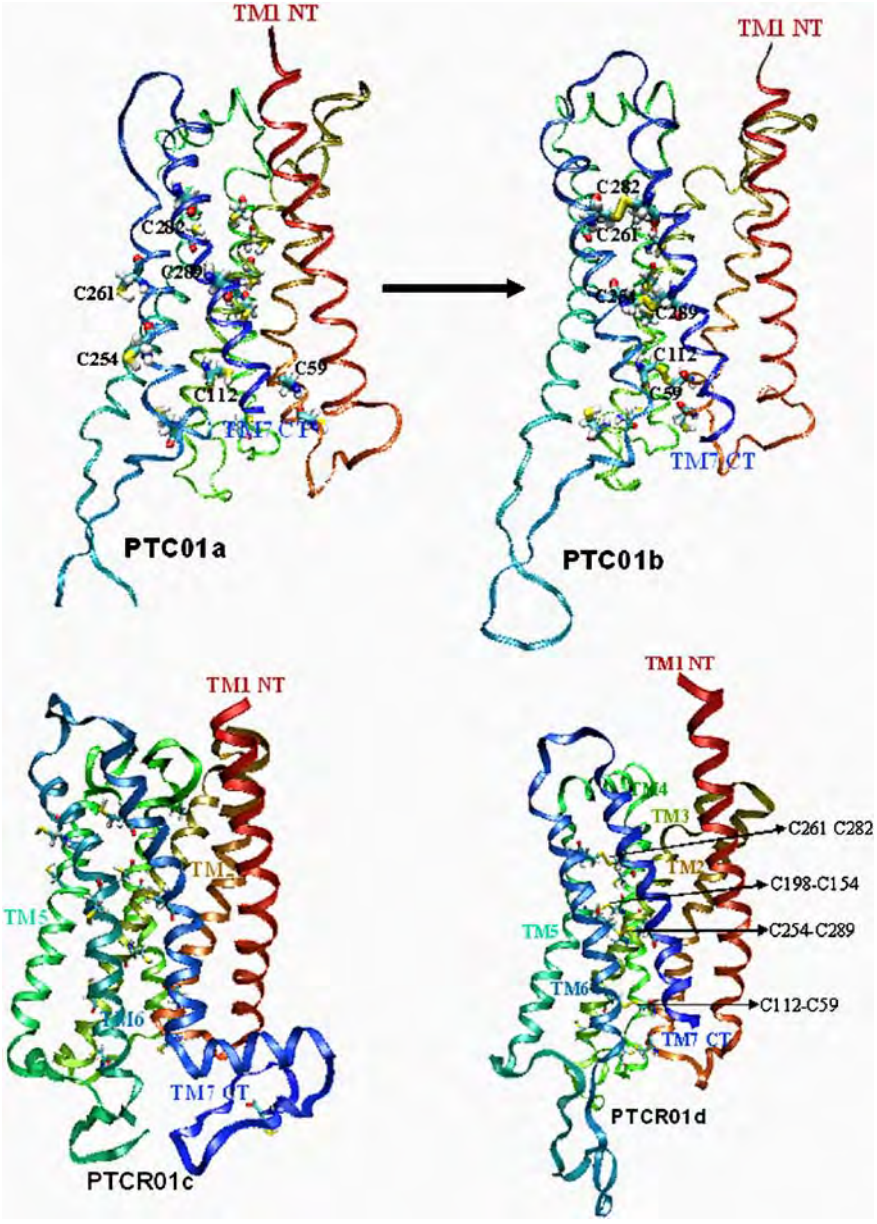

Fig. 2 Predicted 3D structures for phenylthiocarbamide receptor (PTCR). Variant 02 (nontaster) was homology modeled from variant 01 (taster) because they differ in only three amino acids (P49A, A262V, and V296I). The 3D structure (PTCR01a) was built using MembStruk version 3.5, while structure PTCR01b corresponds to PTCR01a, with the helical rotations/translations adjusted to allow for optimal Cys bridges as shown. The homology-derived model (PTCR01c) was built using the experimentally determined structure for rhodopsin (1L9H). 3D model (PTCR01d) is a hybrid homology/MembStruk model (see "Results" for details)

Table 1 Root mean square deviation in coordinates for the alpha Carbon atoms in TM segments among the 3D models built for PTCR

Calpha, 171 aa, TMS, rms (A)	PTCR01a taster	PTCR01b taster	PTCR01c taster	PTCR01d taster
PTCR01a taster	0			
PTCR01b taster	3.2	0		
PTCR01c taster	6.9	7.1	0	
PTCR01d taster	6.5	5.8	5.5	0

(d) (PTCR02 are identical). The binding region found to be most energetically favorable is circled in each structure.

Although the 3D structures obtained using the four approaches are considerably different, two residues were found within 4 Å of the bound ligand for all eight 3D structures: Trp99 (TM3) and Asn103 (TM3). The differences between the structures arise primarily from rotations and translations of some helices. However, the position of TM3, particularly the face with Trp99 and Asn103, seems to determine where PTC binds in all 3D structures.

Location of the SNPs and their distances to bound PTC

Figure 4 shows the TM segments with the SNPs characteristic of PTC tasters and nontasters displayed as van der Waals spheres for the four sets of 3D structures described above. The structural analysis of the SNPs in these 3D models shows that

1. Structures (a) (MembStruk 3.5) and (c) (homology to 1L9H rhodopsin) have positions 262-TM6 facing helix 7, and position 296-TM7 facing helix 6. Therefore, both 3D models suggest that these SNPs are involved in the packing of TMs 6 and 7, and not in the direct binding of ligands.
2. Structures (b) and (c) have 262-TM6 pointing towards the interior of the helical barrel, while 296-(TM7) is pointing towards TM6. For these structures then, 262-TM6 could potentially be directly involved in binding PTC.

The closest SNP to the bound PTC is at position 262 in TM6. The distances between the carbon beta of 262-TM6 and the C1 in PTC are: 8 Å in 3D model (a), 9 Å in 3D model (c), 14 Å in 3D model (b), and 13 Å in 3D model (d). Thus, in all predicted protein–ligand complexes, position

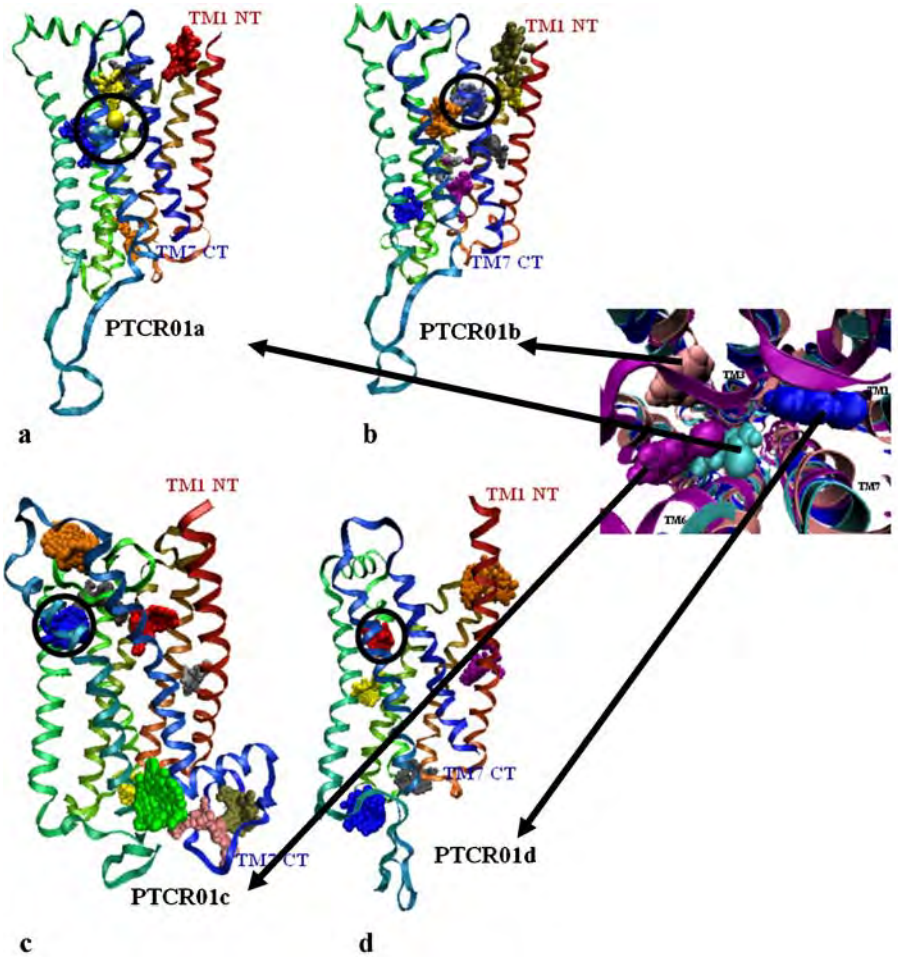

Fig. 3 Location of the predicted binding site for PTC in the PTCR 3D structures. The program ScanBindSite docks and scores multiple configurations of PTC in each of several empty pockets (represented as *sphere clusters with different colors*) throughout the receptor. The probable binding site (*circled sphere cluster*) is defined by the locations of the most energetically favorable receptor. Both variants were independently scanned but only the sites for the taster variant (PTCR01 structures) are shown. The nontaster variant (PTCR02 structures) has the exact same binding site location as PTCR01 for each of the four structure types (**a**)–(**d**)

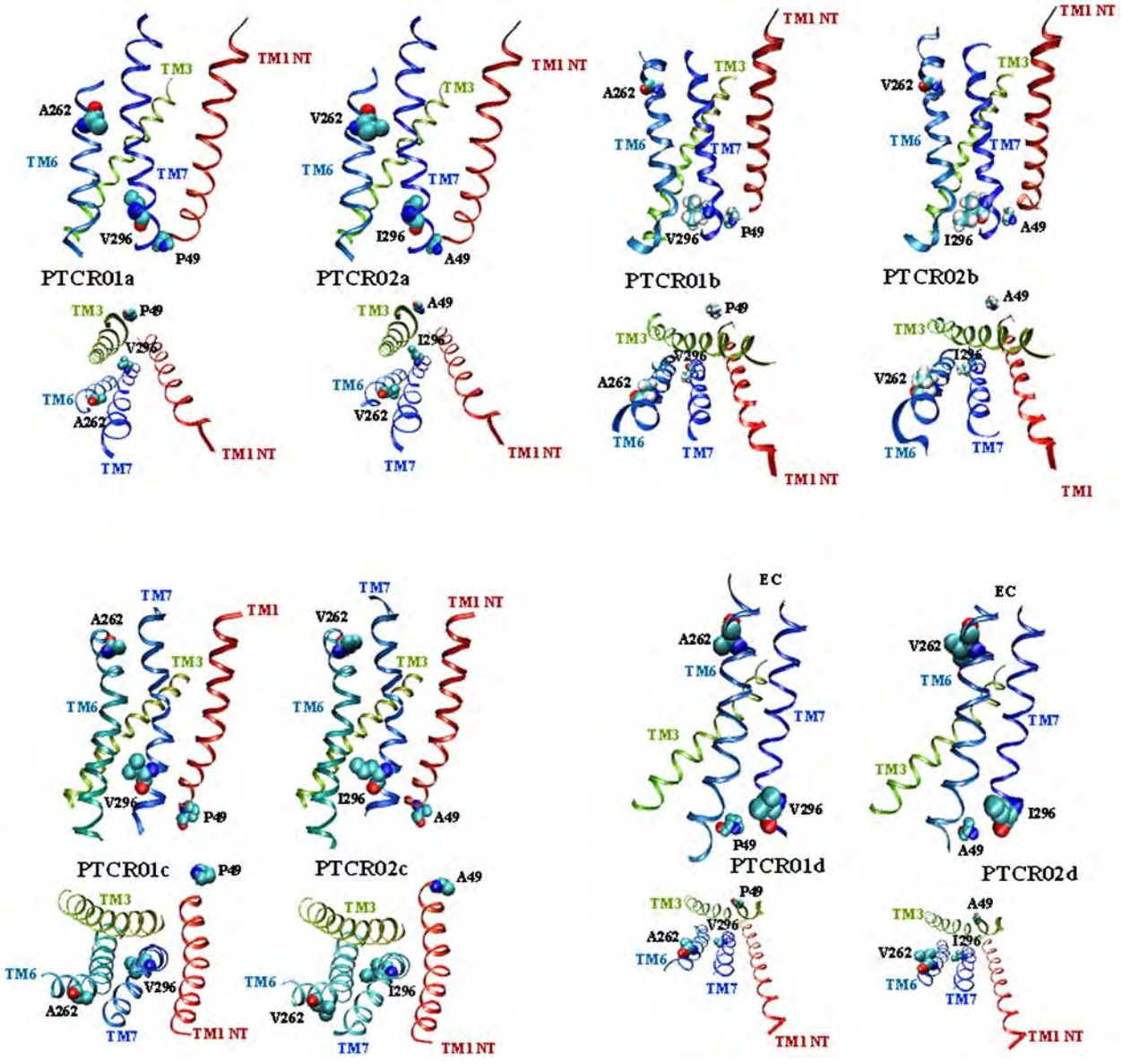

Fig. 4 TM segments with the SNPs characteristic of PTC tasters and nontasters displayed as *van der Waals spheres* for the four types of 3D models built in this work

262-TM6 is too far from PTC to have any significant contribution to the PTC binding energy, and therefore cannot explain the taster/nontaster difference. That is particularly true in the case of structures (b) and (d), not only because of the longer distances but also because these are the only structures that could have an SNP in direct contact with the ligand. Furthermore, the calculated binding energies for the pairs PTCR01 and PTCR02 are nearly the same for each 3D-structure type (a) to (d). Because structures (b) and (d) have one of the three SNPs pointing inside the TM barrel but not within reasonable distance for atomic interaction with PTC, we conclude they are inadequate representations of the PTC receptor. Hence, the rest of our analysis will concern structures (a) (MembStruk 3.5) and (c) (homology-based) only.

The binding mode for PTC in PTCR01a

Residues within 4 Å of the bound ligand in the predicted complexes are shown in Fig. 5. These are Trp99, Met100, Asn103, Gln104, and Leu107 in TM3; Ala263, Phe264, and Val267 in TM6; and Cys282 and Met286 in TM7.

Binding of other bitter ligands to the PTC receptor

We used the calculated binding energies for PTC and 11 additional bitter compounds (atropine, brucine, chloroquine, naringin, quinacrine, quinine, salicin, caffeine, nicotine, epicatechin, and cycloheximide) docked to our 3D models to investigate PTCR01 and PTCR02 further. These predicted binding energies are reported in Table 2

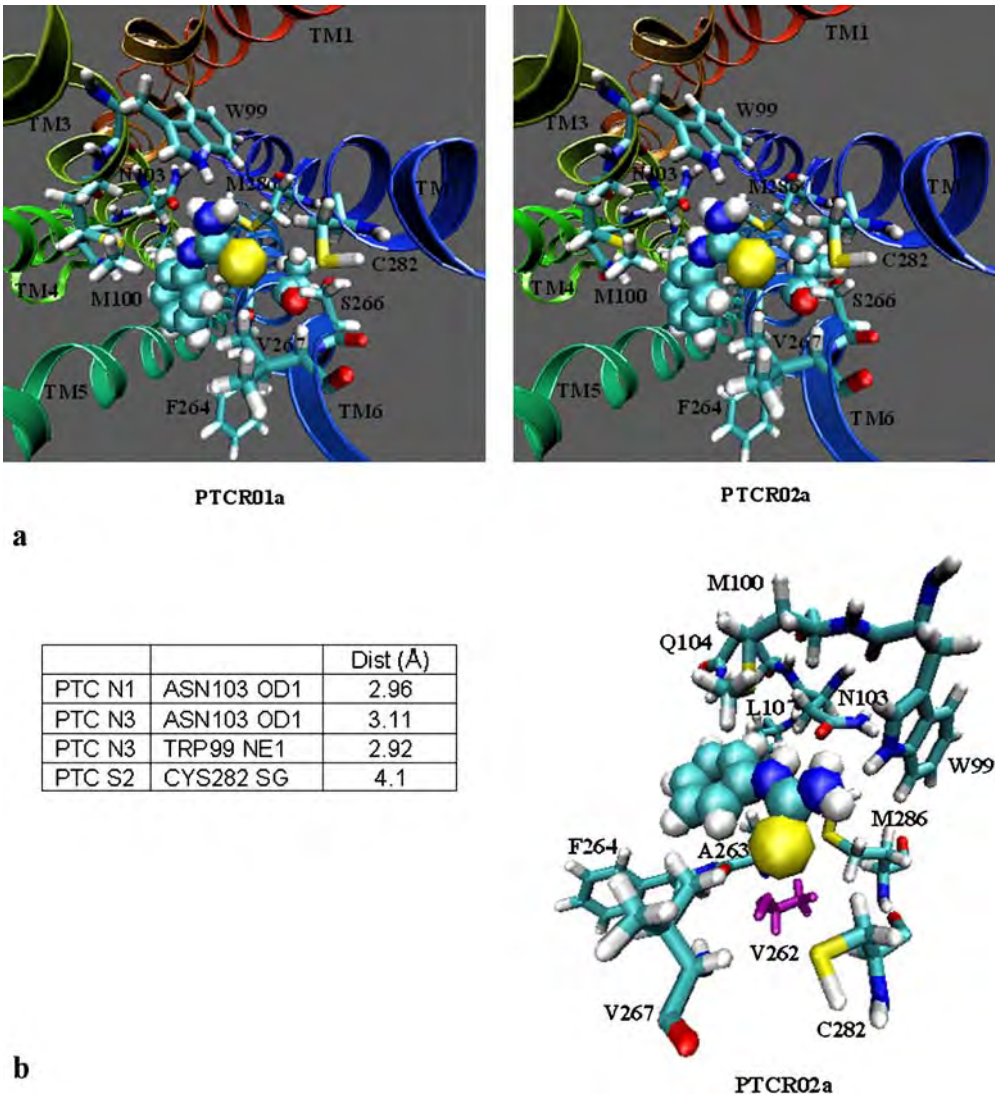

		Dist (Å)
PTC N1	ASN103 OD1	2.96
PTC N3	ASN103 OD1	3.11
PTC N3	TRP99 NE1	2.92
PTC S2	CYS282 SG	4.1

Fig. 5 Predicted 3D structures for phenylthiocarbamide bound to bitter receptor variants PTCR01a (taster) and PTCR02a (nontaster). The figure shows **a** top view from extracellular end and **b** binding mode with residues within 3.5 Å of the bound ligand in *licorice* representation

and Fig. 6. The calculated binding affinities for PTC bound to PTCR01 and PTCR02 show no significant difference in binding between these receptor variants. In addition, no difference in binding affinity is found for the other bitter compounds docked to PTCR01 and PTCR02, as seen in Table 2 and Fig. 6. Furthermore, taste sensitivity to some of the compounds with similar or higher calculated binding affinity to PTCR than PTC has been linked to PTC taster status [9, 11, 12, 32–34].

Discussion

Analysis of PTC sensitivity

These modeling studies emphasize the role of TM6 and TM7 in PTC receptor function. We can now consider how changes in the interactions between TMs 6 and 7 might affect taste sensitivity to PTC. Movement of TM6 has been proposed as part of the structural changes leading to

Table 2 HierDock binding energies (kcal mol^{-1})

Ligand	HierDock binding energy (kcal mol^{-1})	
	PTCR01a	PTCR02a
Naringin	−68.9	−73.5
Salicin	−51.9	−52.0
Epicatechin	−41.1	−37.1
Chloroquine	−35.9	−32.2
Quinacrine	−31.2	−30.3
Quinine	−28.7	−28.0
Atropine	−25.5	−27.1
Phenylthiocarbamide	**−22.1**	**−24.5**
Nicotine	−20.3	−22.0
Caffeine	−14.6	−13.7
Brucine	−4.6	−8.6
Cycloheximide	−0.7	−3.8

Binding energies were calculated as: BindE=E(bound_ligand_in_protein)−E(free_ligand_in_water). These binding energies do not include explicit entropic terms or enthalpic temperature corrections
Values for the known ligand PTC in bold

signaling in GPCRs [35, 36–39]. As shown in Fig. 7, the introduction of bulkier side chains in the nontaster variant alters the packing of TMs 6 and 7, which may render the movement of TM6 (necessary for signaling) more difficult or unattainable. According to our 3D structures, it is plausible that the mutations A262V and V296I would lead to either an inactive receptor or to a reduced function, thus rationalizing the observed taster/nontaster effect.

Our studies lead to three main predictions:

1. The binding affinities of both receptor variants for PTC might be expected to have close or similar energies because the mutations are not directly involved in binding.
2. Nontaster individuals for PTC would also have null or reduced (because one compound may activate multiple bitter receptor types) taste sensitivity for other bitter compounds recognized by the same receptor and with binding affinity similar to PTC. This is supported by psychophysical evidence that PTC nontasters have reduced sensitivity to naringin [12, 33], caffeine [11,

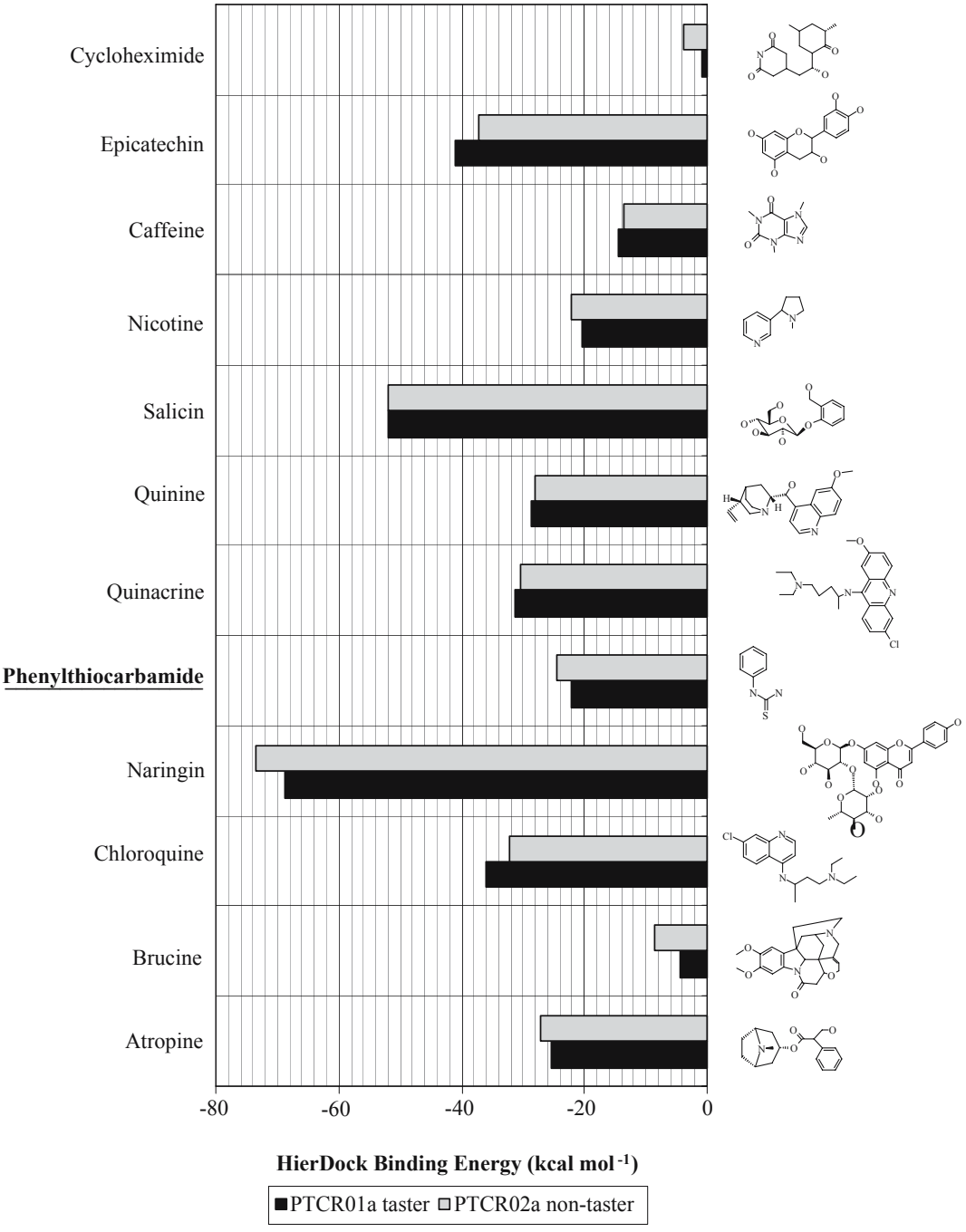

Fig. 6 HierDock-calculated binding affinities (kcal mol^{-1}) for phenylthiocarbamide (PTC), and other tastants docked to PTC receptor variants taster (PTCR01a) and nontaster (PTCR02a)

32, 34], quinine [9, 11], epicatechin, tetralone, urea, sucrose octaacetate, denatonium benzoate, L-phenylalanine, and L-tryptophan [11].
3. Compensatory mutations in TMs 6 and 7 described below could restore nontaster PTCR02 response to PTC.

Considering the close contacts predicted to occur between residues 262-TM6 and 296-TM7 and residues in opposite helices, we suggest mutations that could validate our proposed explanation for the taster/nontaster status of the PTCR variants studied here.

1. The MembStruk model (a) has I285 (TM7) in contact with 262-TM6, and L246 (TM6) and F252 (TM6) opposite to 296-TM7. The mutation of I285 to V, L246 to V, and F252 to I, would change contact to the variant amino acids without causing significant changes in the overall structure of the receptor.
2. The homology-based model (c) points to residues V279 (TM7), which is opposite to 262-TM6), and S248 (TM6) and K247 (TM6), which are both opposite to 296-TM7, as candidates for compensatory mutations. Mutation of V279 to A should improve the packing of I296 (nontaster variant). As for S248 and K247, finding these residues packed against TM7 indicates that the homology-derived 3D structure may have TM6 inappropriately rotated. Polar and charged residues are expected to be either packed against complementary residues or pointing towards the water-accessible center of the barrel.

From the above analysis we conclude that the 3D structures PTCR01a and PTCR02a generated by MembStruk best represent the PTC receptor taster/nontaster variants, and therefore, we will discuss only these structures below.

The involvement of TMs 3, 5, 6, and 7 in GPCR signaling has been documented extensively in the literature [35–42]. It has been suggested [41–43] that interactions between TMs 3, 6, and 7 propagate the signal from the ligand binding site at the extracellular side to the G protein binding site at the intracellular side of the receptor. For constitutively active rhodopsin mutants, the release of interhelical constraints within TMs 3, 6, and 7 produces a structural conformation of the receptor that is more easily activated [44]. The same effect was reported in a recent random mutagenesis study on the opioid receptor [45] showing that certain mutations in TMs 3, 6, and 7 lead to constitutively active receptors. In particular, Decaillot et al. (2003) suggested that the mutations at the intracellular end of TMs 6 and 7 weaken helical packing, allowing the separation of TMs 6 and 7 at the intracellular side.

Our proposed explanation for the PTC taster/nontaster effect associated with the mutations A262V and V296I agrees with the experimental data on constitutively active GPCRs and the signaling model involving TMs 3, 6, and 7. However, instead of mutations causing the activation of receptors without bound ligands, the human PTC receptor appears to have mutations acting in an opposite fashion. In the case of PTCR taster/nontaster variants, the introduction of bulkier side chains at both ends of the TM6/TM7 ladder may increase the attraction between TMs 6 and 7 so that the ligand binding has to provide an additional intermolecular force to activate the receptor. This would probably have the effect of turning off sensitivity to relatively low-affinity ligands like PTC. We note that the proposed steric effects caused by bulkier residues in positions 262-TM6 and 296-TM7 of the nontaster variant may involve residues that

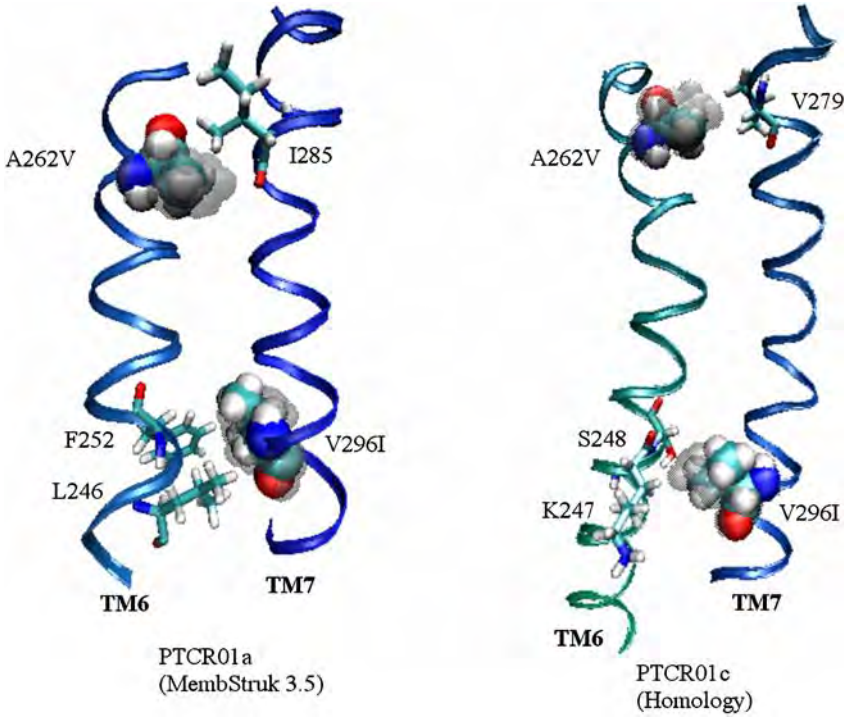

Fig. 7 TMs 6 and 7 with positions 262-TM6 and 296-TM7 shown as *van der Waals spheres*. Amino acids present in the nontaster variant are shown as *gray shadows*. Side chains opposite to the SNP's positions are shown in *licorice*. We propose that compensative mutations in these positions could restore PTC response in the nontaster variant. Note that the residues in close contact to 296-TM7 in the homology-based 3D model PTCR01c are inconsistent with helix–helix packing. The 3D model derived using MembStruk 3.5 seems to be the best representative of the system studied here

come in contact with those positions at some stage of the activation process other than the one represented by our predicted 3D structures.

Bimodal vs modulated taste response

A number of studies support the view that a particular bitter compound may elicit response from one or more bitter receptors present in the same cell, with individual receptors responding to multiple ligands. Covariation patterns found in the sensitivity to certain bitter compounds [11, 12, 31–33] also support a single-ligand/multiple-receptors model which states that a single ligand can activate multiple receptors, as well as a single-receptor/multiple-ligands model. A correlation was found for sensitivity to L-tryptophan, L-phenylalanine, and, to a lesser extent, urea [11, 46], but not between these and PROP. No correlation was found between the ability to taste PROP and taste sensitivity to quinineHCL [47]. Under this view, the bimodal distribution of sensitivity to PTC implies a single receptor type for PTC, while the decreased sensitivity to naringin, caffeine, and other compounds associated with the PTC nontaster variant imply additional receptor types responding to these compounds.

According to our predicted binding profile in Fig. 6, the weak (less negative) binding affinity of cycloheximide and brucine to both PTCR variants suggests that the bitterness of these compounds is not affected by the PTC receptor. On the other hand, compounds predicted as having similar binding affinity to PTC (nicotine, atropine, quinine, quinacrine, and chloroquine) may be perceived as being less bitter by PTC nontasters. However, because these compounds may activate other receptor types, no bimodal response is expected. Compounds we predict as having higher affinity to PTCR (naringin, salicin, and epicatechin) may bind strongly enough so that the resistance to signaling caused by the nontaster SNPs may be overcome. However, sensitivity to naringin, the compound with the strongest affinity to PTCR in our set, has been linked to PTC taster status [8, 12], which suggests that none of the 12 compounds studied here are strong agonists for this receptor.

Conclusion

The MembStruk predicted structure combined with the HierDock predicted binding site provides insight into the activity of the PTC receptor. The small differences between binding affinities calculated for the same compound bound to taster and nontaster variants of PTCR observed for all the docked compounds are consistent with our view that the SNP mutations are not directly involved in ligand binding, but rather in G protein activation. These predicted structures also suggest a number of experiments that can be used to validate the proposed explanation for PTC taste status. We propose that compensatory mutations to PTCR02 that could restore sensitivity to PTC are I285 to V, L246 to V, and F252 to I.

The molecular-level details of the interactions between PTC and its receptor could be further refined by the introduction of algorithms for side-chain rotamer placement and hydrogen bond network optimization during docking. However, even if some details in the predicted structures might benefit from further computational refinement, the comparison to experimental results predicted from the structures would allow corrections in the structures and perhaps improvements in the methods in the most effective way.

Acknowledgements We thank Dr. Susan Sullivan and Dr. John Northup for helpful comments on the manuscript. This work was supported by NIDCD Z01-000046-04, and by NIH-BRGRO1-GM625523, NIH-R29AI40567, and NIH-HD36385. The computational facilities at the Materials and Process Simulation Center (MSC) were provided by a Shared University Research grant from International Business Machines and Defense University Research Instrumentation Program grants from the Army Research Office (ARO) and the Office of Naval Research (ONR). The facilities of the MSC are also supported by the Department of Energy-Advanced Simulation and Computing Program, National Science Foundation, Multidisciplinary Research Initiative - Army Research Office, Multidisciplinary Research Initiative - Office of Naval Research, General Motors, ChevronTexaco, Seiko-Epson, Beckman Institute, and Asahi Kasei.

References

1. Adler E, Hoon MA, Mueller KL, Chandrashekar J, Ryba NJ, Zuker CS (2000) Cell 100:93–702
2. Chandrashekar J, Mueller KL, Hoon MA, Adler E, Feng L, Guo W, Zuker CS, Ryba NJ (2000) Cell 100:703–711
3. Lindemann B (2001) Nature 413:219–225
4. Fox AL (1932) Proc Natl Acad Sci USA 18:115–120
5. Kim UK, Jorgenson E, Coon H, Leppert M, Risch N, Drayna D (2003) Science 299:1221–1225
6. Wooding S, Kim UK, Bamshad MJ, Larsen J, Jorde LB, Drayna D (2004) Am J Hum Genet 74:637–746
7. Fischer R, Griffin F, England S, Garn SM (1961) Nature 191:1328
8. Drewnowski A, Henderson SA, Barratt-Fornell A (2001) Drug Metab Dispos 29:535–538
9. Harris H, Kalmus H (1949) Ann Eugen 15:32–45
10. Barnicot N, Harris H, Kalmus H (1951) Ann Eugen 16:119–128
11. Delwiche JF, Buletic Z, Breslin PA (2001) Percept Psychophys 63:761–776
12. Kameswaran L, Gopalakrishnan S, Sukumar M (1974) Ind J Pharmac 6:134–140
13. Peterson DI, Lonergan LH, Hardinge MG (1968) Arch Environ Health 16:219–222
14. Cannon D, Baker T, Piper M, Scholand MB, Lawrence D, Drayna D, McMahon W, Villegas GM, Caton T, Coon H, Leppert M (2005) Nicotine Tob Res 7:853–858
15. Sultana T, Savage GP, Porter NG (2002) Proc Nutr Soc N Z 27:86–91
16. Floriano WB, Vaidehi N, Singer MS, Goddard WA III, Shepherd GM (2000) Proc Natl Acad Sci USA 97:10712–10716
17. Vaidehi N, Floriano WB, Trabanino R, Hall SE, Freddolino P, Choi EJ, Zamanakos G, Goddard WA III (2002) Proc Natl Acad Sci USA 99:12622–12627
18. Trabanino RJ, Hall S, Vaidehi N, Floriano WB, Goddard WA III (2004) Biophys J 84:1904–1921

19. Floriano WB, Nagarajan V, Zamanakos G, Goddard WA III (2004) J Med Chem 47:56–71
20. MDL Information Systems Inc, http://www.mdli.com
21. Tripos Inc, http://www.tripos.com
22. Gasteiger J, Marsili M (1980) Tetrahedron 36:3219–3228
23. Mayo SL, Olafson BD, Goddard WA III (1990) J Phys Chem 94:8897–8909
24. Accelrys Inc, http://www.accelrys.com
25. Vriend G (1990) J Mol Graph 8:52–56
26. MacKerell AD, Bashford D, Bellott M, Dunbrack RL, Evanseck JD, Field MJ, Fischer S, Gao J, Guo H, Ha S, Joseph-McCarthy D, Kuchnir L, Kuczera K, Lau FTK, Schlenkrich M, Smith JC, Stote R, Straub J, Watanabe M, Wiorkiewicz-Kuczera J, Yin D, Karplus M (1998) J Phys Chem B 102:3586–3616
27. Brady GP Jr, Stouten PFW (2000) J Comput Aided Mol Des 14:383–401
28. Freddolino PL, Yashar M, Kalani S, Vaidehi N, Floriano WB, Hall SE, Trabanino RJ, Kam VW, Goddard WA III (2004) Proc Natl Acad Sci USA 101:2736–2741
29. Floriano WB, Vaidehi N, Goddard WA III (2004) Chem Senses 29:269–290
30. Thompson JD, Higgins DG, Gibson TJ (1994) Nucleic Acids Res 22:4673–4680
31. Palczewski K, Kumasaka T, Hori T, Behnke CA, Motoshima H, Fox BA, Le Trong I, Teller DC, Okada T, Stenkamp RF, Yamamoto M, Miyano M (2000) Science 289:739–745
32. Hall MJ, Bartoshuk LM, Cain WS, Stevens JC (1975) Nature 253:442–443
33. Drewnowski A, Henderson SA, Shore AB (1997) Am J Clin Nutr 66:391–397
34. Bartoshuk LM (2000) Chem Senses 25:447–460
35. Farrens DL, Altenbach C, Yang K, Hubbell WL, Khorana HG (1996) Science 274:768–770
36. Sheikh SP, Zvyaga TA, Lichtarge O, Sakmar TP, Bourne HR (1996) Nature 383:347–350
37. Gether U, Lin S, Ghanouni P, Ballesteros JA, Weinstein H, Kobilka BK (1997) EMBO J 16:6737–6747
38. Dunham TD, Farrens DL (1999) J Biol Chem 274:1683–1690
39. Medkova M, Preininger AM, Yu NJ, Hubbell WL, Hamm HE (2002) Biochemistry 41:9962–9972
40. Schmidt C, Li B, Bloodworth L, Erlenbach I, Zeng FY, Wess J (2003) J Biol Chem 278:30248–30260
41. Pauwels PJ, Wurch T (1998) Mol Neurobiol 17:109–135
42. Gether U (2000) Endocr Rev 21:90–113
43. Okada T, Ernst OP, Palczewski K, Hofmann KP (2001) Trends Biochem Sci 26:318–324
44. Rao VR, Oprian DD (1996) Annu Rev Biophys Biomol Struct 25:287–314
45. Decaillot FM, Befort K, Filliol D, Yue S, Walker P, Kieffer BL (2003) Nat Struct Biol 10:629–636
46. Keast RS, Breslin PA (2002) Chem Senses 27:123–131
47. Schifferstein HNJ, Frijters JER (1991) Chem Senses 16:303–317